N74-

Paper No. 29

TRANSIENT FREQUENCY EFFECTS IN PIEZOELECTRIC QUARTZ CRYSTALS CAUSED BY INCIDENT THERMAL RADIATION

D. A. Wallace, *Celesco Industries Inc., Costa Mesa, California*

ABSTRACT

An analytical and experimental program examined step function and cyclic thermal irradiance of piezoelectric crystals. Metal crystal electrodes with different α/ϵ ratios as well as dielectric over-coated electrodes were tested.

INTRODUCTION

Quartz Crystal Microbalances (QCM's) are widely used to measure small mass changes resulting from condensible efflux depositing upon a piezoelectric crystal. The condensing mass results in a predictable crystal vibrational frequency change which has been treated theoretically and experimentally by various investigators. To relate crystal frequency changes to mass changes, however, other potential frequency effecting phenomena must be considered. The relationship between crystal frequency and equilibrium quartz crystal temperature has been thoroughly studied for various crystallographic cuts and over a broad temperature range. With a full understanding of this frequency-equilibrium temperature relationship, QCM's can be produced with essentially zero beat frequency change with temperature by using two crystals with matched temperature characteristics and exposing only one crystal to mass flux.

An important frequency change producing parameter which has been inadequately studied, however, is transient or steady state incident thermal radiation. QCM's positioned on spacecraft so as to be exposed to solar radiation and thin film monitors subjected to IR heating by evaporative sources are examples of QCM's in this incident radiation environment. This study considered various theoretical thermal models for the prediction of heat flow through the quartz plate and the resultant stress producing thermal gradients which could result in frequency shifts completely independent of any equilibrium temperature effects. An experimental program provided input information for the thermal modeling and verification of the analytical predictions.

Analytic Study

Using the case of constant heat flux suddenly applied at the surface of a plate at equilibrium, the heat pulse within the

plate produced by sudden exposure to solar radiant flux can be analyzed.

The solution for the temperature variation within the plate with sudden constant heat flux applied to one side of the plate and with radiative heat rejection from the other plate surface is found in Reference 1.

Evaluating the eigen functions for the quartz crystal case indicates a high thermal conductivity through the plate compared to the heat rejected by radiation from the back surface of the plate. The calculated time for the heat pulse to pass through the crystal is much less than one second.

In the case of the crystals being studied, a metallic electrode is deposited onto a piezoelectric quartz crystal with a diameter ratio (d_e/d_q) of approximately one-half. The metal electrode is absorptive to the irradiation, however the quartz has a high transmittance or in practice is shielded from the radiant flux.

In actuality then the crystal case is much closer to the case of a hollow cylinder with suddenly applied heat at the inner diameter (Figure 1) since the heat absorbed by the metal electrode passes very quickly through the quartz and then proceeds to flow radially throughout the plate --the crystal thickness to diameter ratio being 1/80.

The plate diffusivity (α) controls the time required to reach steady state temperature gradient in the plate.

$$\alpha = \frac{k}{\rho c_p} = 8.3 \times 10^{-3} \text{ cm}^2/\text{sec at } 25^\circ\text{C}$$

Therefore, for the typical one-half inch diameter crystal with a one-quarter inch diameter electrode the transient heat flow parameter is

$$\frac{\alpha \tau}{l^2} = 0.09$$

A unity value of $\alpha \tau / l^2$ indicates steady state has approximately been reached. Therefore, approximately 10 seconds are required to establish a steady state temperature gradient in the crystal. Once this gradient is established the bulk temperature of the quartz rises at a rate dependent upon its specific heat but with the initial gradient superimposed upon it.

It has been established experimentally that radial thermal gradients with heat flow from the center of the crystal to the periphery result in plate stresses that produce increases in frequency. Imposing a radiant heat flux onto the crystal thus imvariably will initially result in a frequency rise which is dependent upon the heat actually absorbed by the plate and the quartz thermal diffusivity. The transient which follows this initial frequency increase is controlled by the equilibrium temperature coefficient of the crystal and the thermal resistance of the conductive joint through which heat must leave the

quartz plate.

Figure 2 illustrates this behavior for radiant flux to a crystal operating in a temperature region of negative equilibrium temperature coefficient. If the crystal is essentially insulated, i. e. very poor joint conductivity, the initial frequency rise may eventually be more than compensated by a drop in frequency resulting from bulk plate temperature rise. As the thermal joint conductance increases the bulk plate temperature is prevented from rising as high and thus the compensating drop in frequency is lessened. Likewise, a reduced temperature coefficient due to either a changed crystallographic cut or to operation in a more favorable temperature range, will reduce the secondary frequency drop. Discontinuance of the radiant flux results in a drop in frequency of the same magnitude as the radial gradient induced rise with subsequent plate cooling.

The effect of the equilibrium temperature coefficient on transient response is shown for various temperatures in Figure 3. In this figure, case 1 corresponds to the high negative temperature coefficient condition just discussed and case 2 illustrates the effect of decreased temperature coefficient as the turnover point is approached. In case 3, the radial gradient induced frequency rise and the bulk temperature induced frequency increase are complementary.

EXPERIMENTAL PARAMETERS

The parameters chosen for general verification of the thermal model were:

1. Heat absorbed by crystal. The α/ϵ ratio of the electrode was varied by use of both vapor deposited gold and aluminum electrodes as well as aluminum electrodes with a 8000Å overcoating of SiO_x.
2. Heat rejected by crystal. The crystals were mounted in supportive rings which provided varying degrees of thermal conductance for heat transfer from the crystal. Crystals were peripherally mounted using RTV 118, and RTV 566 approximately 0. 002" thich, as well as a spring loaded mechanical mount with four helical springs providing 300 grams of force on the crystal edge which was seated on a #16 polished gold plated stainless steel ring. All three of these mounting techniques have been previously flight qualified.
3. Equilibrium temperature coefficient. Crystals with 10 MHz fundamental frequency and two different crystallographic crystal cuts were used ($\phi_1 = 35^\circ\ 18'$, $\phi_2 = 37^\circ\ 03'$) to obtain widely differing temperature coefficients at a particular temperature.
4. Cyclic heat input. The effect of a 6 rpm rotation into and out of a one solar constant irradiance was also examined.

TEST SETUP

The test program was conducted in Celesco Industries'

three foot diameter by four foot long diffusion pumped vacuum chamber. The test setup within the chamber is shown in Figure 4. The crystals under test, were supported from a temperature controlled heat sink which facilitated testing at various temperatures.

The crystals were surrounded by liquid nitrogen cooled surfaces essentially eliminating background radiation to the unit. The crystal mount and shield are shown in Figure 5. The test crystal oscillator/mixer electronics and reference crystal were positioned below the test rig in a constant temperature environment to avoid extraneous temperature effects.

The simulated solar irradiance was provided by a GE 500 watt, 3400°K color temperature photo spot lamp projected into the radiation shielded crystals by a liquid nitrogen cooled front surface mirror. Simulation of the solar flux during 6 rpm rotation cycle was provided by a shaped aluminum plate which rotated through the field of the lamp as illustrated in Figure 6. The transient frequency effects produced by the photo spot lamp are comparable to effects produced by true solar spectrum flux as discussed in Appendix A.

The crystal frequency was displayed on a Model 3735A HP frequency counter, and analoged and recorded on a Model 7100B Mosely strip chart recorder. A thermistor attached to the ring of the crystal was used to monitor the crystal mount temperature.

A Hy-Cal Engineering Hy-Therm Pyrheliometer Model P-8400-B-050120 was used as the basic heat flux calibration gage. The Hy-Cal calibration was based upon one solar constant of 1398 watts/m^2 rather than the newly accepted 1353 watts/m^2. To this extent the data will be conservative.

TEST PROCEDURE

All tests were performed at pressures below 10^{-6} torr. The crystals were exposed to two separate intervals of continuous one solar constant irradiance and a period of 6 rpm cyclic irradiance at 0.5, 1, and 1.5 solar constants. The lower limit of test temperature varied with the crystal mount configuration. Previous steady state testing indicated stress producing phase changes for RTV 118 at -65°C, RTV 566 at -110°C and no noticeable change to -196°C for the spring mount. The RTV 118 mount was thus tested only to -50°C, the RTV 566 to -80°C and the spring mount to -140°C to avoid any extraneous mount induced effects.

TEST RESULTS

The transient response of the various test configurations, as a function of temperature is shown in Figure 7 and the quasi-steady state frequency shift (measured after the initial transient) in Figure 8.

Generally the frequency transient behavior was as described in the analysis section i. e. initial frequency rise followed by a temperature coefficient or thermal joint conductivity controlled increase or decrease in frequency.

Crystal Mount Parameter

As indicated in Figures 7 and 8 the spring mount resulted in a more nearly insulated crystal mount with the temperature coefficient becoming the controlling parameter as the crystal was able to change bulk temperature readily. Thus at 25°C with a large negative temperature coefficient (aluminum electrode crystals) the initial increase is quickly reversed by a frequency decrease induced by the rising crystal bulk temperature frequency. The same crystal (Al + S_iO_x) mounted on RTV 566 recovered only fractionally from the initial rise indicating higher thermal conductivity through the mounting material. At temperatures below the turn-over point, the positive temperature coefficient resulted in a large additive frequency increment to the initial rise in the spring mount whereas a much lower rise would be expected with the RTV 566 with its higher thermal conductivity. This assumption is supported by the slope of the RTV 566 data.

The importance of joint thermal conductivity is illustrated also by the difference in frequency shift between the gold electrode RTV 566 and the RTV 118 mount. The evidently lower conductivity of the RTV 118 may be influenced by the lack of gold plating on these particular crystal mounting rings and thus lower heat transfer from the RTV 118 joint to the eventual heat sink. However, on an area basis it appears that the RTV must be the main contributor to poor heat conduction.

Absorptance Parameter

The gold electrode crystals have a higher absorptance than aluminum for the photo spot's radiation spectrum as discussed in Appendix A and therefore the initial frequency shift is higher as shown in Figures 7 and 8. However, the slope of the gold electrode crystal's temperature coefficient curve is so small compared to that of the aluminum electrode crystal (~1/14 at 25°C and -50°C) that very little effect of the bulk plate temperature change is observed. As discussed in Appendix A, the radiation source used in this test produces frequency transients on the aluminum electrode crystals which should clearly match transients produced by actual solar radiation, however, considerably larger transient effects are expected for gold electrodes in solar radiation (Figure 10). Reference 2 reports 200 Hz frequency shifts for crystals and mounts identical to the gold RTV 118 configuration reported here for several QCM's on Skylab.

The S_iO_x coated crystals experience greater frequency shifts than the uncoated crystals at all temperatures indicating a higher absorptivity than the base metal electrode. If the S_iO_x has the same absorption characteristics as S_iO, the increased

absorptivity is apparent from the data of Figure 10. Additionally, the S_iO_x is applied by evaporation resulting in a porous coating with mass density of only one-half the bulk density of fused silica. Reference 3 indicates higher absorptance does result from highly anisotropic layers.

The general nature of the cyclic (6 rpm) thermal radiation induced transients is shown in Figure 3 at several different temperature coefficient conditions. Since at the simulated 6 rpm the crystal is only exposed to a sine function of one solar constant irradiance for five seconds per cycle and the radial gradient induced frequency rise time is ten seconds, a general "chopping" of the steady flux transient is expected and is confirmed by Figure 9. In this graph the amplitude of the frequency variation is shown as well as the cycle's displacement from the zero radiation ($\Delta f = 0$) frequency.

CONCLUSIONS

In order to minimize frequency transients due to solar irradiance, QCM crystals should have the following characteristics:

1. Metal electrode material should have low absorptance for solar radiation. Aluminum in this case being superior to gold.
2. S_iO_x overcoatings on crystals increase frequency shifts and therefore should be avoided if possible.
3. High thermal conductivity of the crystal to mounting ring joint will reduce frequency shifts.
4. Cyclic rotation in and out of the solar irradiance will reduce the frequency shift amplitude if the rotation period is shorter than approximately ten seconds.

REFERENCES

1. Conduction of Heat in Solids - H. S. Carslaw and J. C. Jaeger, Clarendon Press.
2. Quartz Crystal Microbalance Contamination Monitors on Skylab - A Quick-look Analysis, R. Naumann, W. Moore, D. Nisen, W. Russell and P. Tashbar. NASA MSFC, June 8, 1973.
3. Effects of Surfaces on the Intrinsic Radiation Properties of Dielectrics - J. C. Klein, Symposium on Thermal Radiation of Solids NASA SP-55.
4. Ultraviolet Radiation, Koller, Wiley Press.

ACKNOWLEDGEMENTS

Mr. D. Bergquist spent many hours performing diligently these tests as well as assisting in the analysis. Mr. K. Rogers provided as usual many helpful suggestions in the heat transfer analysis.

APPENDIX A

THE PHOTO SPOT LAMP AS A SOLAR IRRADIANCE SIMULATOR

The argument for the validity of a 'solar simulator' test using any type of lamp source hinges not upon how well the lamp reproduces the solar spectrum but rather on how well the effects of radiation of a solar spectral nature impinging upon surfaces of interest are duplicated by a lamp of a different spectral character.

In the present test a GE 500 watt, 3400°K color temperature photo spot lamp was used to produce one solar constant (1398 watts/m^2) of irradiance at the test station. To produce this irradiance level the lamp was operated at only 58 volts. Reference 4 indicates reduction to one-third filament temperature would be expected for this reduction from the 110 volt rated voltage. The peak irradiance thus should be reduced from approximately 1 micrometer wavelength to 2.5 micrometers by Wien's displacement law. Measurements with a Jarrell Ash Monochromator did not verify this prediction. This instrument has reduced sensitivity in the near IR region, however no spectral differences were measurable for the two lamp voltage settings. The most that can be said then is that blackbody radiation at between 1000°K and 3400°K is incident on the crystals. This is not to say that either blackbody spectral radiance curve fully describes the radiation emitted by the lamp. The lamp's glass envelope has a 2.7 micrometer cutoff on the IR side of the curve as seen in Figure 10, thus only wavelengths less than 2.7 micrometer are emitted by the lamp.

The materials to be considered in this test are aluminum and gold vacuum deposited on 3μ grit polished natural quartz and silicon dioxide vacuum deposited to a 8000Å thickness over the aluminum. In the case of vacuum deposited aluminum films, Figure 10 indicates a relatively small change in reflectance as the spectrum shifts from solar to the near IR. Transient thermal effects in aluminum coated quartz plates irradiated with the Photo Spot lamp should be very nearly the same then as the effects produced by true solar radiation. Very nearly the same amount of heat energy will enter the plate for the same irradiation level. This is not true for gold electrodes. Even if the lamp temperature is on the high side (3000°K) only a fraction of the energy is at wavelengths less than .5 micrometers where gold has a high absorptance (Figure 10). Solar radiation on the other hand is peaking in this region. Test results on gold electrodes using this lamp thus can be used on a comparative basis only.

The S_iO_2 is actually deposited as a S_iO_x which has slightly higher absorptance in the Photo Spot spectrum as previously discussed and somewhat larger absorbtance in the UV portion of solar spectrum which is missing in Photo Spot lamp.

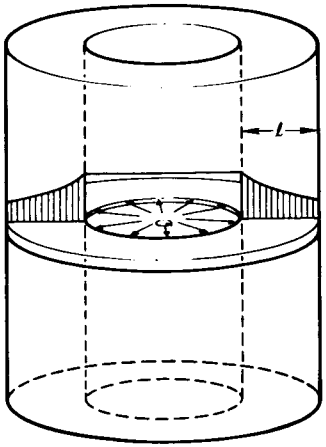

Fig. 1—Hollow Cylinder Heat Transfer Model

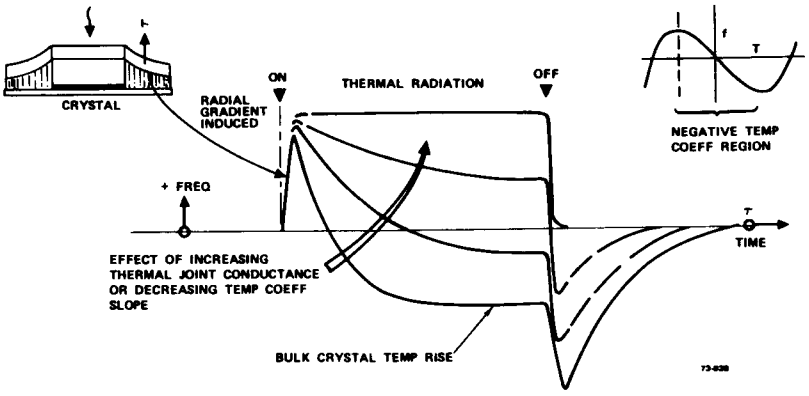

Fig. 2—Crystal Transient Response for Negative Equilibrium Temperature Coefficient

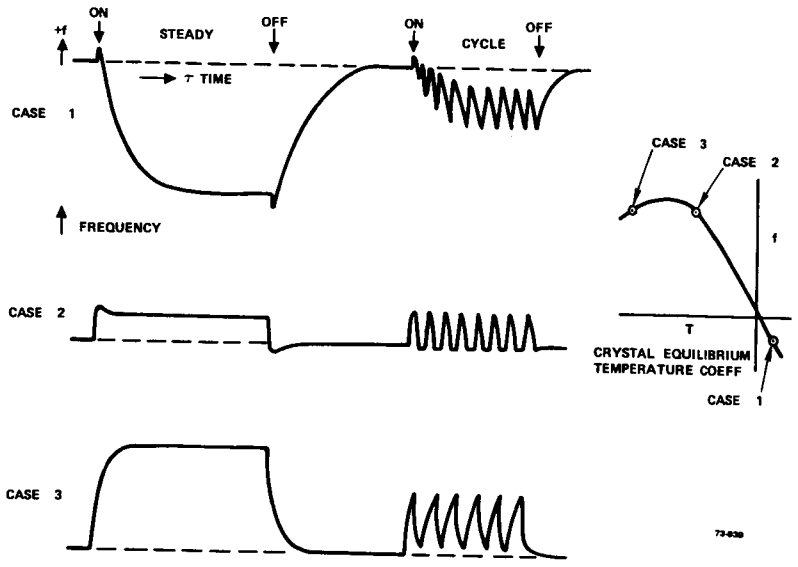

Fig. 3—Transient Frequency Response as a Function of Temperature Coefficient

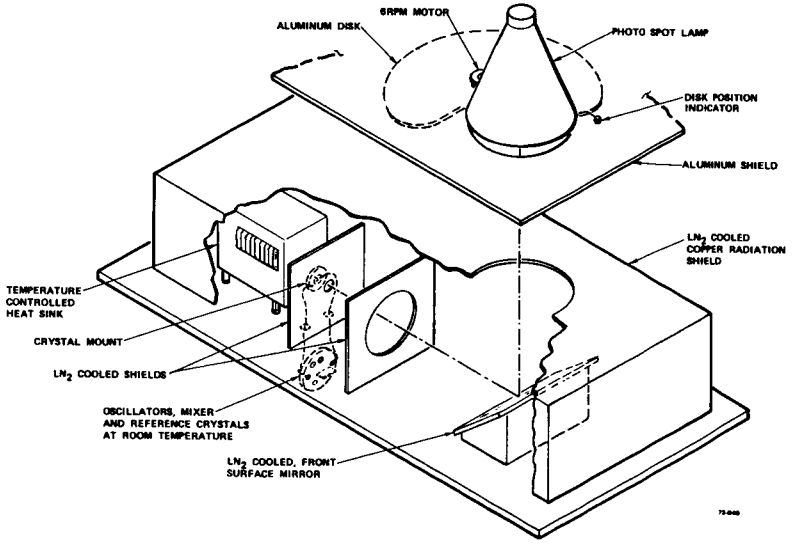

Fig. 4—Test Setup

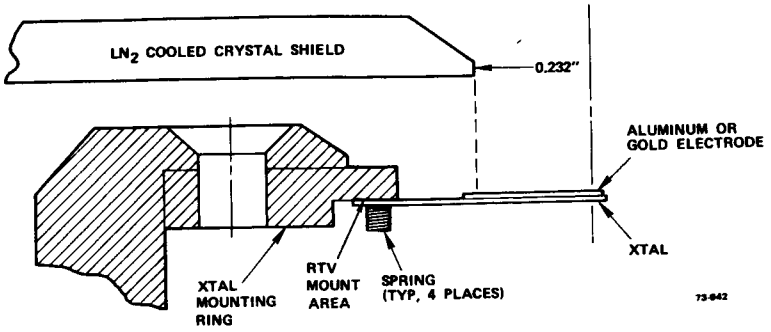

Fig. 5—Aperature for Crystal Irradiance

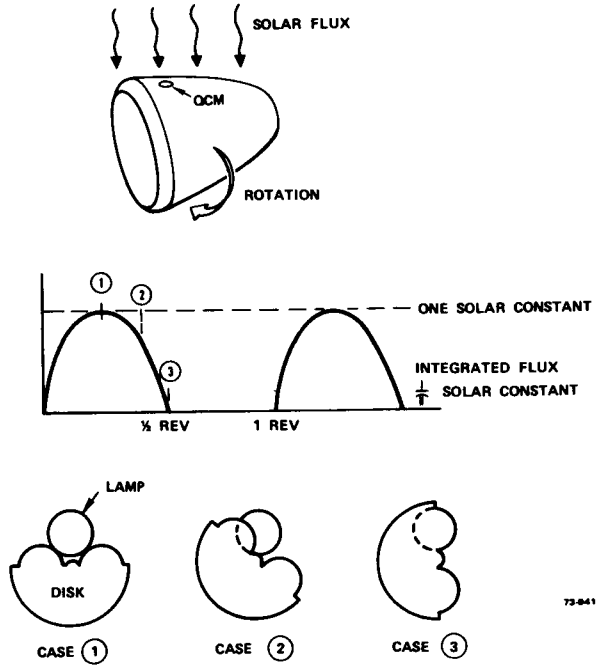

Fig. 6—Rotation Simulation

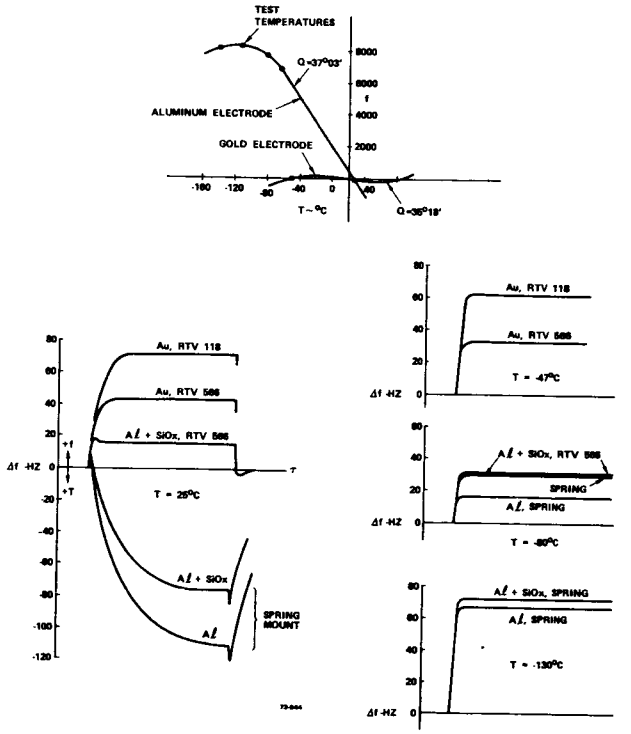

Fig. 7—Crystal Frequency Response to Irradiance at Various Temperatures

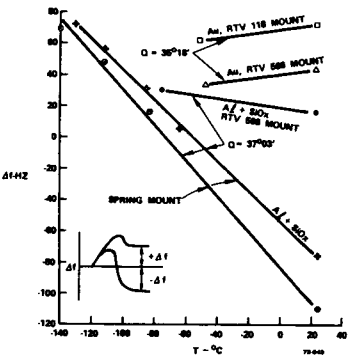

Fig. 8—Effect of Electrode Material and Mount Configuration on Transient Amplitude

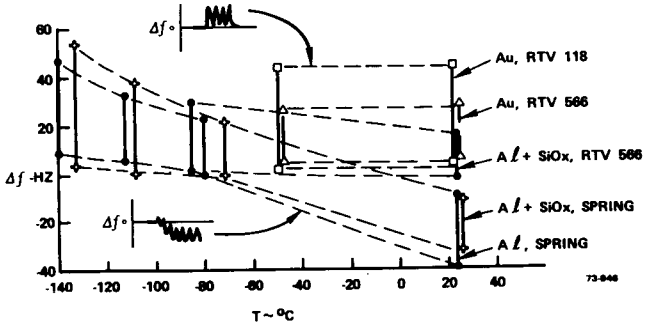

Fig. 9—Effect of Simulated 6rpm Rotation on Transient Amplitude

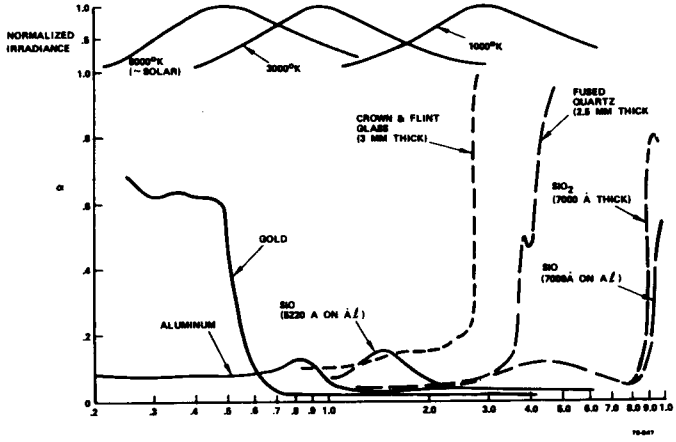

Fig. 10—Wavelength λ Micrometers